Eur Phys J A (2004) **19**, s01, 229–237
Digital Object Identifier (DOI) 10.1140/epjad/s2004-03-038-4

EPJ A direct
electronic only

$b\bar{b}b\bar{b}$ production in proton-proton and proton-nucleus collisions at the CERN LHC

A. Del Fabbro and D. Treleani

Dipartimento di Fisica Teorica dell'Università di Trieste and INFN, Sezione di Trieste, Strada Costiera 11, Miramare-Grignano, I-34014 Trieste, Italy

Received: 27 Jul / Accepted: 14 Nov 2003 /
Published Online: 6 Feb 2004 –

Abstract. Given the large parton luminosities, sizable rate of events, with several pairs of b-quarks produced contemporarily by multiple parton interactions, are foreseen in hadronic and nuclear collisions at very high energies. We compare the different contributions to $b\bar{b}b\bar{b}$ production, due to single and double parton scatterings, in pp and in pA collisions at the CERN LHC within the acceptance of the ALICE and of the LHCb detectors.

PACS. 14.20.Dh – 13.40.Gp – 21.10.Ft

1 Introduction

The production mechanism of heavy quarks in hadronic collisions is non trivial and also the simplest observable quantity, the integrated inclusive cross section, cannot be easily reproduced in perturbation theory [1]. Comparisons with the experimental data of the D0 Collaboration [2] at TEVATRON indeed have shown that the NLO pQCD calculations in α_S [3] underestimate the cross section by a factor $\sim 2, 3$.

A complementary approach to heavy quarks production, which keeps explicitly into account that transverse momenta and virtualities of the interacting partons become increasingly important in the kinematical regime of $s \gg m_b^2 \sim \hat{s} \gg \Lambda^2$, and includes terms at every order in α_S in the calculation of the cross section, is the k_t-factorization, where the interaction is factorized into un-integrated structure functions and off shell matrix elements [4,5,6]. Phenomenologically the k_t-factorization is not inconsistent with HERA and TEVATRON data and allow one to reproduce both the value of the integrated inclusive cross section and various differential distributions, including the correlation in the azimuthal angle between the produced b quarks, where different approaches are less successfully compared with experiment [7].

Interestingly, although the value of the integrated inclusive cross section cannot be obtained trivially, one may find several cases where the overall effect of higher order corrections amounts to a simple rescaling of the lowest order parton model result. Several distributions, derived either using the k_t-factorization approach or by working out the cross section at the NLO pQCD, are in fact rather similar (apart form normalization) to those obtained with a simplest lowest order calculation [8]. In a few cases, the whole effect of higher order corrections is hence (approximately) reduced to a single numerical value, the K factor:

$$K = \frac{\sigma(b\bar{b})}{\sigma_{LO}(b\bar{b})} . \tag{1}$$

where $\sigma(b\bar{b})$ is the actual inclusive cross section and $\sigma_{LO}(b\bar{b})$ the result of the lowest order calculation in pQCD.

Although the expected inclusive cross section of b production is hence still pretty uncertain at LHC energies, all estimates point in the direction of rather large values because of the high parton luminosity [9]. The fairly large flux of partons make it also plausible to expect a sizable rate of events, where two or more $b\bar{b}$ pairs are produced contemporarily by different partonic collisions in a single pp interaction [10]. One of the reasons of interest in the production of multiple pairs of b quarks is that such a process allows to generate and study a completely new sector of hadon spectroscopy, namely double heavy barions and double b tetraquarks [11,12]. We think that it's hence interesting to estimate the production rates of multiple $b\bar{b}$ pairs at the LHC, comparing the two possible production mechanisms, multiparton interactions and the more conventional single parton collision process [13].

We limit our considerations to the simplest cases, where the whole effect of higher order corrections is taken into account by the overall normalization factor. Given the lack of information on higher order corrections in the $2 \to 4$ processes, we assume that the K factors of the $gg \to b\bar{b}b\bar{b}$ and of the $gg \to b\bar{b}$ processes are equal. The $gg \to b\bar{b}$ process is worked out in the k_t-factorization approach, fixing the input parameters by comparing with the TEVATRON data. The cross section is then extrapolated

at LHC energies, identifying a few differential distributions where the effect of higher order corrections reduces to a simple rescaling of the lowest order result. The value of the K-factor derived in this way is used to renormalize the double $(gg \to b\bar{b})^2$ and the single $gg \to b\bar{b}b\bar{b}$ parton scattering cross sections, which are evaluated by working out all Feynman diagrams at order α_S^4.

2 $b\bar{b}$ cross section at TEVATRON and LHC and K-factor

In the k_t-factorization approach the $b\bar{b}$ production cross section is expressed as [4,5]

$$\sigma(pp \to b\bar{b}) = \int \frac{d^2q_{t1}}{\pi}\frac{d^2q_{t2}}{\pi}\, dx_1 dx_2\, f(x_1, q_{t1}, \mu) \times f(x_2, q_{t2}, \mu)\, \hat{\sigma}(x_1, q_{t1}; x_2, q_{t2}; \mu) \quad (2)$$

where $f(x, q_t, \mu)$ is the unintegrated structure function, representing the probability to find a parton with momentum fraction x, transverse momentum q_t at the factorization scale μ, while $\hat{\sigma}$ is the off-shell partonic cross section of the process $g^*g^* \to Q\bar{Q}$.

To evaluate the inclusive cross section we use two different prescriptions for constructing the k_t-distributions from the usual integrated parton densities. The first is based on the conventional DGLAP evolutions equations [14], with virtual corrections re-summed in the survival probability factor $T_a(k_t^2, \mu^2)$ [15]. For the second prescription we follow [16], where the un-integrated structure functions are obtained from the leading order BFKL equation and are expressed as the convolution of the collinear gluon densities $G(x, \mu^2)$ with the universal function $\mathcal{G}(x, k_t^2, \mu^2)$:

$$\mathcal{F}(x, k_t^2, \mu^2) = \int_x^1 d\xi\, \mathcal{G}(\xi, k_t^2, \mu^2)\, G\Big(\frac{\xi}{x}, \mu^2\Big) \quad (3)$$

The weight factors $\mathcal{G}(\xi, k_t^2, \mu^2)$ are known in double-logarithmic approximation and depend on the quantity $\bar{\alpha}_s = 3\alpha_s/\pi$, which in the BFKL formalism is a fixed quantity, related to the pomeron intercept $\alpha(0) = 1 + \Delta$, with $\Delta = 4\bar{\alpha}_s \log 2$. Following [17] we take $\Delta = 0.35$.

To obtain the functions $\mathcal{F}(x, k_t^2, \mu^2)$ we use the parton distributions set GRV94 [18] with factorization scale $\mu_F^2 = \hat{s}$, while the cross section at the lowest order in pQCD is evaluated with the MRS99 parton distributions [19], with factorization and renormalization scale equal to the transverse mass of the b-quark. Comparing the total cross sections, we obtain $K \sim 5.5$.

In Fig. 1 the integrated cross section of $b\bar{b}$ production is plotted as a function of the minimum value of the transverse momentum p_t^{min} of the b-quarkat both at TEVATRON($\sqrt{s} = 1.8$TeV) and at LHC($\sqrt{s} = 14$TeV). The dotted curves represent the cross section derived using the unintegrated gluon structure function, according with the BFKL prescription of (4), whereas the dashed lines are evaluated by using the prescription in (3). The continuous lines represent the result of the lowest order calculation multiplied by the K factor. At TEVATRON

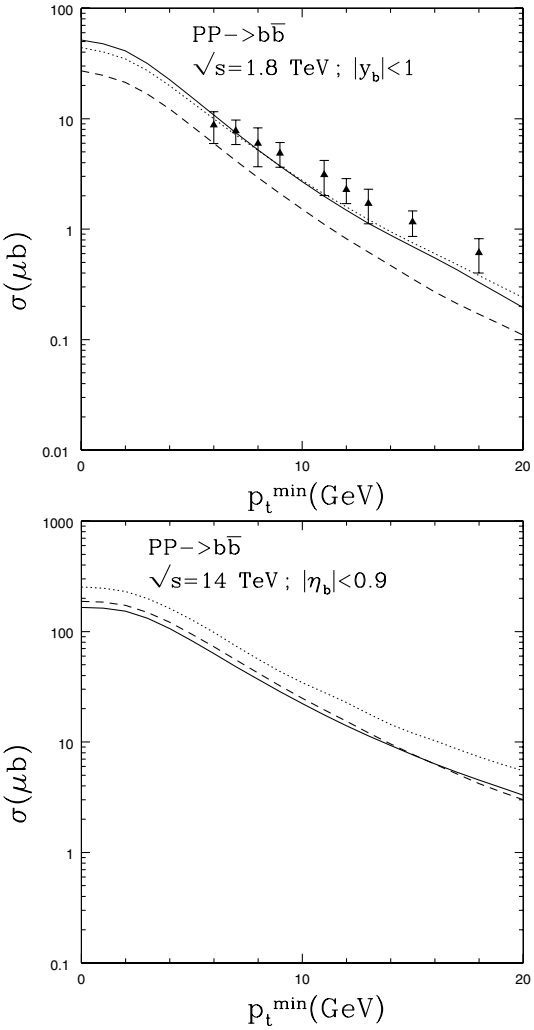

Fig. 1. $p\bar{p} \to b\bar{b}$ production cross section as a function of p_t^{min} at $\sqrt{s} = 1.8TeV$, with the b-quark within the rapidity range $|y_b| < 1$, experimental data from [2], and at $\sqrt{s} = 14$ TeV with the b-quark within the pseudo-rapidity range $|\eta| < 0.9$

energy the b-quark distributions are within the rapidity interval $|y| < 1$ and are compared with the D0 experimental data [2]. The same distributions, extrapolated at LHC energy, are plotted as a function of p_t^{min} within the pseudorapidity interval $|\eta| < 0.9$, corresponding to the acceptance of the ALICE detector.

In Fig. 2 the rapidity(y) and pseudorapidity(η) distributions are shown, normalized to one and within $|\eta| < 0.9$. The continuous histograms are the result of the lowest order calculation, whereas the dashed histograms represent the distributions evaluated with the k_t-factorization approach.

As one may see in the cases considered the whole effect of higher orders reduces to a simple rescaling.

3 $b\bar{b}b\bar{b}$ cross section

We will compare the two competing mechanisms of $b\bar{b}b\bar{b}$ production, the leading order QCD $2 \to 4$ [20] and the

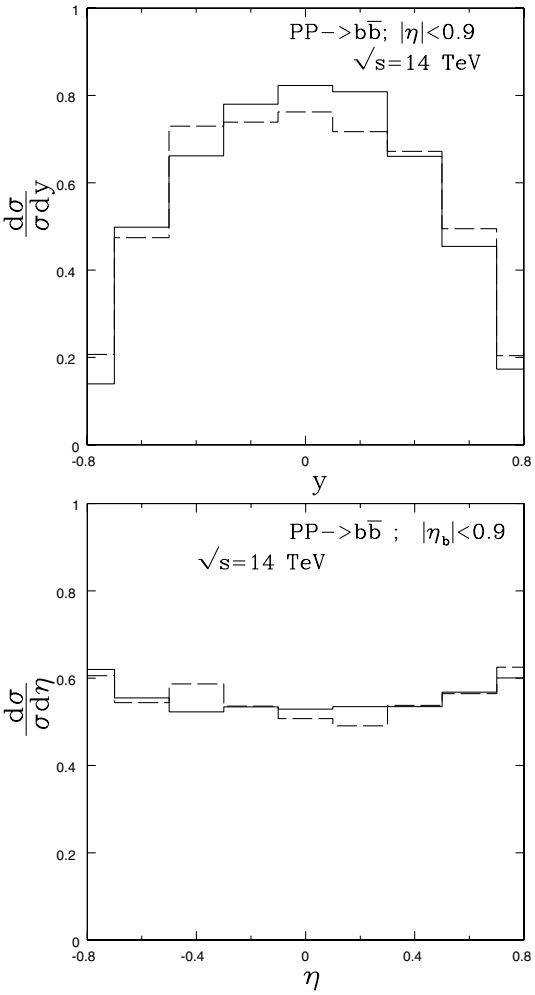

Fig. 2. Normalized rapidity (y) and pseudorapidity (η) distributions for $b\bar{b}$ production at ALICE with the k_t factorization approach (*dashed histograms*) and at the lowest order in pQCD multiplied by the K-factor (*continuous histograms*)

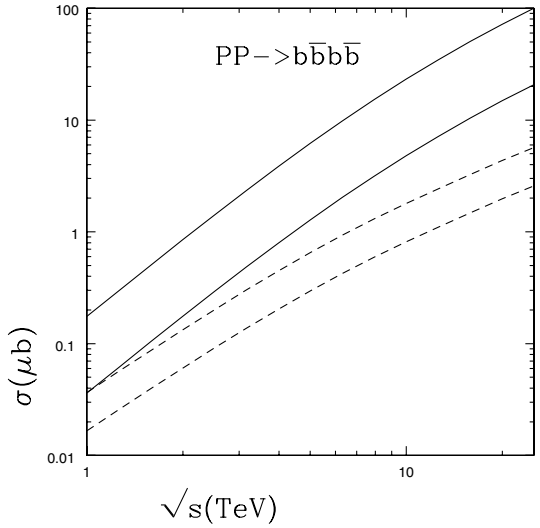

Fig. 3. $b\bar{b}b\bar{b}$ total cross section as a function of centre of mass energy. *Lower curves* $K = 2.5$, *higher curves* $K = 5.5$

double parton scattering $(2 \to 2)^2$ [21], in proton-proton collisions in the kinematical range of the ALICE and of the LHCb detectors, namely at center-of-mass energies of 5.5 and 14 TeV, within the pseudorapidity regions $|\eta| < 0.9$ and $1.8 < \eta < 4.9$, down to very low transverse momenta.

For the leading order in α_s single scattering subprocesses, one needs to evaluate 14 Feynman diagrams for each flavor in the initial state, for quarks initiated process, and 76 diagrams for gluon fusion. We generate the matrix elements of the partonic amplitudes with MadGraph [22] and HELAS [23]. As a value of the bottom quark mass we take $m_b = 4.6$ GeV and we use the MRS99 parton distributions [19]. The resulting cross section is then multiplied by the K factor, obtained as described in the previous section, while the multi-dimensional integrations are performed by VEGAS [24].

To evaluate the double parton scattering cross section the input two-body parton distribution functions $\Gamma(x_1, x_2, s)$ is needed [10]. Here $x_{1,2}$ are the fractional momenta of the two partons belonging to the same hadron and s their distance in transverse space. We make the usual simplifying assumption of neglecting all parton correlations in fractional momenta, so we factorize the two-body parton distribution as

$$\Gamma(x_1, x_2, s) = G(x_1)G(x_2)F(s) \tag{4}$$

where $G(x)$ are the usual one-body parton distributions and $F(s)$ is a function normalized to 1 and representing the parton pair density in transverse space. The double scattering cross section is hence written as [25]

$$\sigma_D(b\bar{b}; b\bar{b}) = \frac{1}{2}\sum_{ij} \Theta^{ij}\sigma_i(b\bar{b})\sigma_j(b\bar{b}) \tag{5}$$

where the indices i, j label the different cases where each $b\bar{b}$ pair is originated either by a $q\bar{q}$ annihilation, discriminating the cases of sea and valence, or by two gluons and $\sigma_i(b\bar{b})$ represents the inclusive cross sections for $b\bar{b}$ production in a hadronic collision, the index i labelling a definite parton process. The weight factors Θ^{ij} have dimension an inverse cross section and result from integrating the product of the two-body parton distributions in transverse space, while the factor 1/2 is a consequence of the symmetry of the expression for exchanging i and j. The dependence of Θ^{ij} on the indices i, j accounts for the possibility, for different pairs of partons in the hadron, to be characterized by different values of their relative average transverse distance [25,21].

When looking at the experimental analysis of double parton scatterings [26,27,28] one finds the cross section expressed as:

$$\sigma_D = \frac{m}{2}\frac{\sigma_S(A)\sigma_S(B)}{\sigma_{eff}} \tag{6}$$

where $m = 1$ if the two parton processes A and B are identical, while $m = 2$ if they are different and σ_S is the single scattering inclusive cross section. The relation may

be obtained by neglecting the dependence of the factors Θ^{ij} in (5) on the different elementary processes.

As the dominant contribution to $b\bar{b}b\bar{b}$ production at the LHC is gluon fusion, for the present purposes the sum in (5) may be approximated well by a single term, while the scale factor should not be strongly different from the value observed in the CDF experiment. Hence for the double scattering cross section we use:

$$\sigma_D(b\bar{b}b\bar{b}) = \frac{\sigma(b\bar{b})^2}{2\sigma_{eff}}\,. \tag{7}$$

where for σ_{eff} we take the value reported by CDF, $\sigma_{eff} = 14.5$ mb. Notice that since σ_D is proportional to σ_S^2, the effect of higher order corrections is enhanced on σ_D:

$$\begin{aligned} \sigma_S &= K\,\sigma_S^{LO} \\ \sigma_D &= K^2\,\sigma_D^{LO} \end{aligned} \tag{8}$$

where $\sigma_{S,D}^{LO}$ refers to the lowest order expressions of the cross section.

4 Results for $b\bar{b}b\bar{b}$ production in pp collisions

In Fig. 3 the cross section for $b\bar{b}b\bar{b}$ production is shown as a function of the c.m. energy. The continuous curves refer to the double parton scattering contribution, while the dotted curves to single scattering. In both cases the lower curve is evaluated with $K = 2.5$, while the higher curve with $K = 5.5$, which are the typical estimates of the NLO-pQCD and the result of our calculation within the k_t-factorization approach.

In Fig. 4 the two contributions to the integrated cross section, are plotted as a function of p_t^{min}, the minimum value of the transverse momenta of the b quarks (which are required to be all inside the pseudorapidity interval $|\eta| < 0.9$), at 14 and 5.5 TeV. The continuous curves refer to the double parton scattering contribution, while the dotted curves to single scattering. The double parton cross section decreases faster with p_t^{min} than the single parton cross section, the two contributions are of the same order at $p_t^{min} = 8-10$ GeV. Pseudorapidity, and rapidity distributions at 14 TeV are plotted in Fig. 5, where continuous and dashed histograms have the same meaning as in the previous cases.

In Fig. 6 we plot the pseudorapidity (η) distributions at $\sqrt{s} = 14$ TeV, requiring both b-quarks to be in the pseudorapidity interval $1.8 < \eta < 4.9$, corresponds to the acceptance of the LHCb detectort. In the same figure we also compare the single and double parton scattering contributions, integrated within the rapidity acceptance of the LHCb, as a function of p_t^{min}.

The overall indication is that double parton scatterings dominate the $b\bar{b}b\bar{b}$ integrated cross section by a large factor, both in the central rapidity region and at the larger rapidity values of the LHCb experiment. In both cases the contribution of the single parton scattering term becomes important only after applying cuts to the transverse momenta of the order of 8-10 GeV.

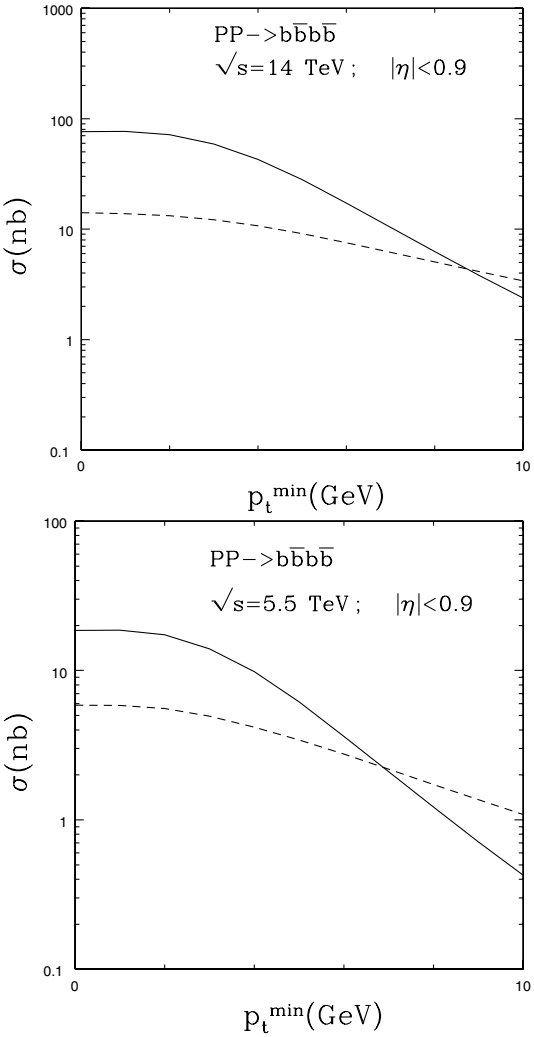

Fig. 4. $b\bar{b}b\bar{b}$ production cross section at $\sqrt{s} = 14$ TeV and at $\sqrt{s} = 5.5$ TeV as a function of p_t^{min} with all the four b-quarks in the pseudo-rapidity interval $|\eta| < 0.9$

5 $b\bar{b}b\bar{b}$ production in pA collisions

All production rates are significantly enhanced in proton-nucleus collisions, which may offer considerable advantages for studying multiparton interactions [29]. Quite in general [30,31] the expression of the double parton scattering cross section to produce two $b\bar{b}$ pairs is given by

$$\begin{aligned} \sigma_A^D(b\bar{b},b\bar{b}) \;&= \frac{1}{2}\sum_{ij}\int \Gamma_p(x_i,x_j;s_{ij})\hat{\sigma}(x_i,x_i')\hat{\sigma}(x_j,x_j') \\ &\times\; \Gamma_A(x_j',x_j';s_{ij})dx_i dx_i' dx_j dx_j' d^2 s_{ij}, \end{aligned} \tag{9}$$

where the index A refers to the target nucleus, the indices i, j to the different kinds of partons that annihilate to produce a $b\bar{b}$ pair and the factor $1/2$ is a consequence of the symmetry of the expression for exchanging i and j.

The most suitable conditions are those where the nuclear distributions are additive in the nucleon parton distributions. In such a case one may express the nuclear

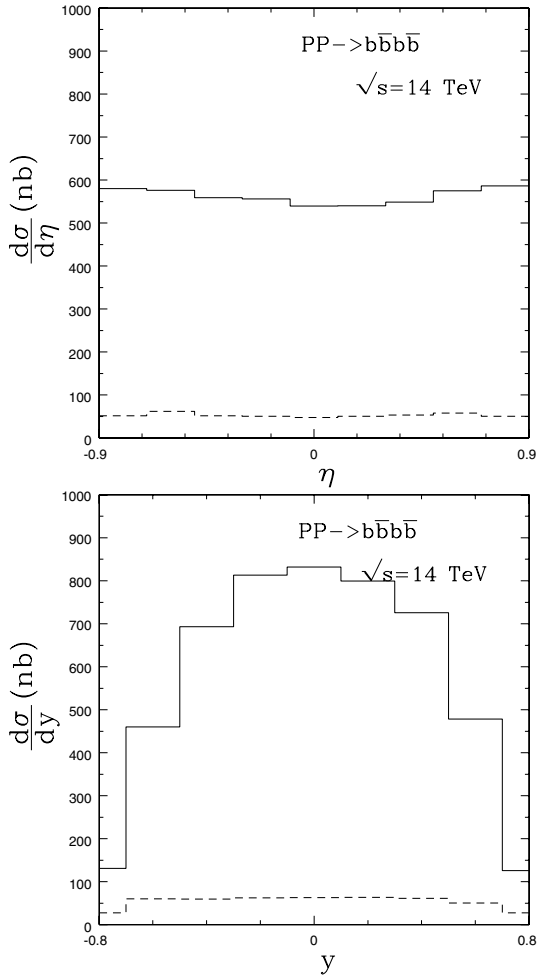

Fig. 5. $b\bar{b}b\bar{b}$ production with the two equal sign b-quarks in the pseudo-rapidity interval $|\eta_b| < 0.9$. η-distributions and y_b-distributions at $\sqrt{s} = 14$ TeV. The *continuous histograms* refer to the contribution of double parton scatterings while the *dashed histograms* to single parton scattering

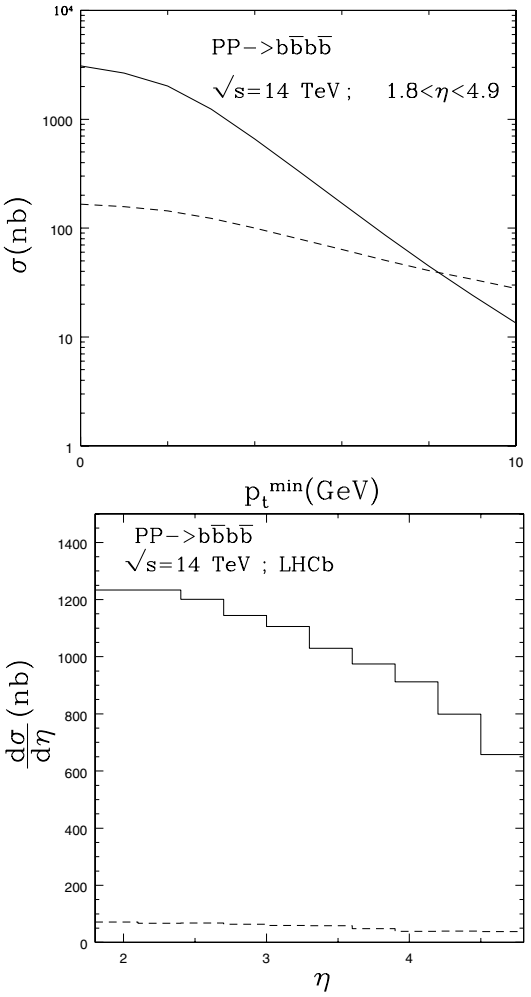

Fig. 6. $b\bar{b}b\bar{b}$ production with the two equal sign b-quarks in the pseudo-rapidity interval $1.8 < \eta < 4.9$ at $\sqrt{s} = 14$ TeV. Production cross section as a function of p_t^{min} and η. The *continuous line and histogram* refer to the contribution of double parton scatterings while the *dashed line and histogram* to single parton scattering

parton pair density, $\Gamma_A(x_j', x_j'; s_{ij})$, as the sum of two well defined contributions, where the two partons are originated by either one or by two different parent nucleons:

$$\Gamma_A(x_i', x_j'; s_{ij}) = \Gamma_A(x_i', x_j'; s_{ij})\Big|_1 + \Gamma_A(x_i', x_j'; s_{ij})\Big|_2 \quad (10)$$

and correspondingly $\sigma_A^D = \sigma_A^D|_1 + \sigma_A^D|_2$. The two terms $\Gamma_A|_{1,2}$ are easily expressed in terms of the nuclear nucleon's density by introducing the transverse parton coordinates $B \pm \frac{s_{ij}}{2}$, where B is the impact parameter of the hadron-nucleus collision. One may write

$$\Gamma_A(x_i', x_j'; s_{ij})\Big|_{1,2} = \int d^2B \gamma_A\Big(x_i', x_j'; B + \frac{s_{ij}}{2}, B - \frac{s_{ij}}{2}\Big)\Big|_{1,2} \quad (11)$$

where $\gamma_A|_{1,2}$ are given by

$$\gamma_A\Big(x_i', x_j'; B + \frac{s_{ij}}{2}, B - \frac{s_{ij}}{2}\Big)\Big|_1 = \Gamma_N(x_i', x_j'; s_{ij}) T(B)$$

$$\gamma_A\Big(x_i', x_j'; B + \frac{s_{ij}}{2}, B - \frac{s_{ij}}{2}\Big)\Big|_2 = G_N(x_i') G_N(x_j') \times T\Big(B + \frac{s_{ij}}{2}\Big) T\Big(B - \frac{s_{ij}}{2}\Big) \quad (12)$$

with $T(B)$ is the nuclear thickness function, normalized to the atomic mass number A and G_N nuclear parton distributions divided by the atomic mass number.

The first term in (10) gives a simple rescaling of the double parton distribution of a isolated nucleon:

$$\Gamma_A(x_i', x_j'; s_{ij})\Big|_1 = \Gamma_N(x_i', x_j'; s_{ij}) \int d^2B T(B) \quad (13)$$

The resulting contribution to the cross section is the same as in a nucleon-nucleon interaction, enhanced by the atomic mass number factor A:

$$\sigma_A^D\Big|_1 = A \sigma_N^D \quad (14)$$

The $\sigma_A^D|_2$ term involves two different target nucleons in the integration on the relative transverse coordinate s_{ij}:

$$\int ds_{ij} \Gamma_p(x_i, x_j; s_{ij}) T\Big(B + \frac{s_{ij}}{2}\Big) T\Big(B - \frac{s_{ij}}{2}\Big) \qquad (15)$$

In the limit where the hadron radius is much smaller than the nuclear radius one may approximate

$$T\Big(B \pm \frac{s_{ij}}{2}\Big) \simeq T(B) \qquad (16)$$

The integrations on s_{ij} and on B are hence decoupled. One obtains:

$$\sigma_A^D\Big|_2 = \frac{1}{2} \sum_{ij} \int G_p(x_i, x_j) \hat{\sigma}(x_i, x_i') \hat{\sigma}(x_j, x_j') \times G_N(x_i') G_N(x_j') dx_i dx_i' dx_j dx_j' \int d^2B T^2(B), \qquad (17)$$

where

$$G_p(x_i, x_j) = \int d^2 s_{ij} \Gamma_p(x_i, x_j; s_{ij}) \qquad (18)$$

Remarkably the two terms $\sigma_A^D\Big|_1$ and $\sigma_A^D\Big|_2$ have very different properties. In fact the correct dimensionality of $\sigma_A^D\Big|_1$ is provided by transverse scale factors related to the *nucleon* scale, cfr. (5),(14). The analogous dimensional factor in $\sigma_A^D\Big|_2$ is provided by the *nuclear* thickness function, which is at the second power, being two the target nucleons involved in the interaction.

As pointed out in [29], while on general grounds σ_A^D depends both on the longitudinal and transverse parton correlations, the $\sigma_A^D\Big|_2$ term depends solely on the longitudinal momentum fractions x_i, x_j so that, when the $\sigma_A^D\Big|_2$ term is isolated, one has the capability of measuring the longitudinal and, a fortiori, also the transverse parton correlations of the hadron structure in a model independent way.

The additivity of the nuclear structure functions may not be a bad approximation for a sizable part of the kinematical regime of bottom quarks production at the LHC. In the case of a central calorimeter with the acceptance of the ALICE detector ($|\eta| < 0.9$), the average value of momentum fraction of the initial state partons, in a $pp \to b\bar{b}b\bar{b}$ process, is $\langle x \rangle \approx 6 \times 10^{-3}$. By introducing a cut in the transverse momenta of the b quarks of 5 GeV one obtains $\langle x \rangle \approx 10^{-2}$, while a cut of 20 GeV in p_t, within the same pseudorapidity range, gives $\langle x \rangle \approx 2 \times 10^{-2}$. If considering a more forward detector, as LHCb ($1.8 < \eta < 4.9$), the average value of momentum fraction is $\langle x \rangle \approx 5 \times 10^{-2}$. Deviations from additivity at low x are less than 10% for $x \geq 2 \times 10^{-2}$ [32] and, although increasing with the atomic mass number, non additive corrections are at most a 20% effect, on the considered kinematical regime.

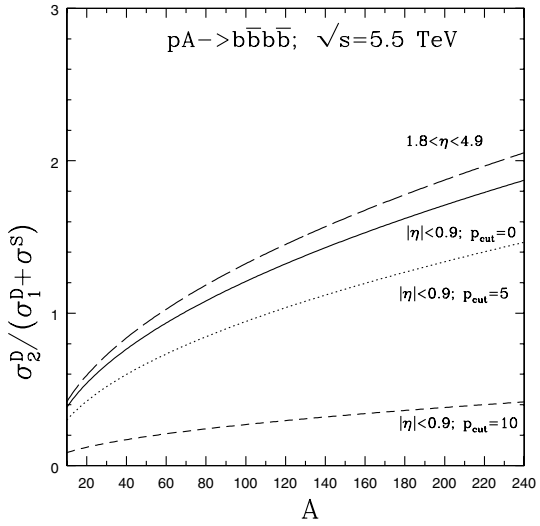

Fig. 7. Relative weights of the terms with "anomalous" and "usual" A-dependence in the double scattering cross section for $b\bar{b}b\bar{b}$ production

6 Results for $b\bar{b}b\bar{b}$ production in pA collisions

A major result is that the effects, induced by the presence of the nucleonic degrees of freedom in double parton scatterings with a nuclear target, cannot be reduced to the simple shadowing corrections of the nuclear parton structure functions, which cause a decrease of the cross section as a function of A. In the case of double parton collisions, the main effect of the nuclear structure is represented by the presence of the $\sigma_A^D|_2$ term in the cross section, which scales with a different power of A as compared to the single scattering contribution, producing a additive correction to the cross section.

The 'anomalous' dependence of the double parton scattering cross section, as a function of the atomic mass number, is emphasized in Fig. 7, where the ratio $\sigma_2^D/(\sigma_1^D + \sigma^S)$ is plotted as a function of A. The ratio represents the contribution to the cross section of the processes where two different nuclear target nucleons are involved in the interaction, scaled to the contribution where only a single target nucleon is involved. The dependence on the atomic mass number of the latter terms is the same of all hard processes usually considered, where nuclear effects may be wholly absorbed in the shadowing corrections to the nuclear structure functions. The contribution to the cross section of the σ_2^D term is, on the contrary, "anomalous", involving two different target nucleons in the interaction. The ratio above hence represents the relative weights of the "anomalous" to the "usual" contributions to the double parton scattering cross section on a nuclear target. The plots in Fig. 7 refer to the cases $1.8 \leq \eta \leq 4.9$ and $|\eta| \leq .9$, with different cuts on the transverse momenta of the produced b-quarks ($p_{cut} = 0, 5, 10$ GeV/c).

The different contributions to the cross section due to interactions with a single or with two different target nucleons, are shown in Fig. 8, in the case of a central calorimeter. The upper figure shows the cross section as

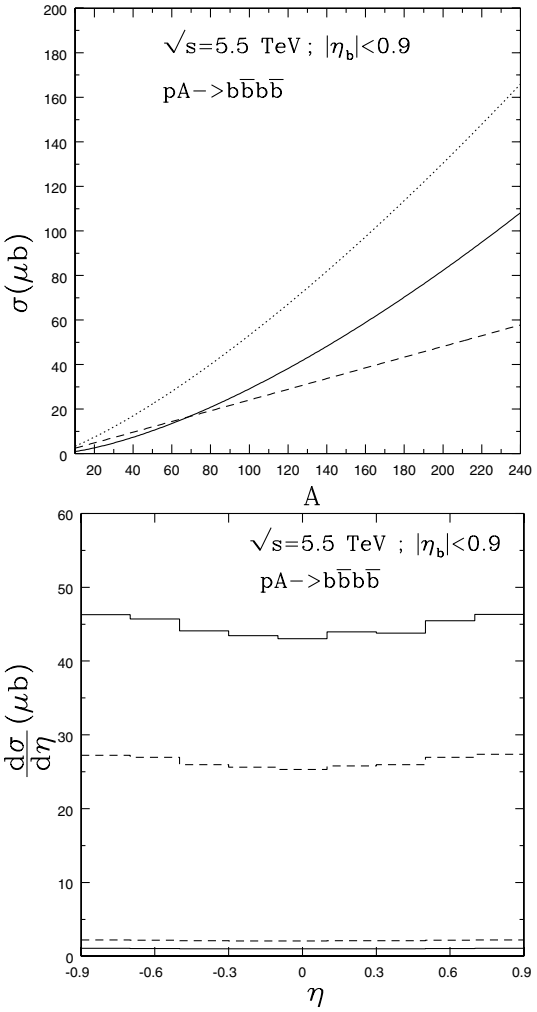

Fig. 8. Different contributions to the cross section for $b\bar{b}b\bar{b}$ production, in a central calorimeter. *Upper figure:* cross section as a function of A of the one-nucleon (*dashed line*) and of the two nucleons (*continuous line*) terms. The *dotted line* is the sum of the two terms. *Lower figure:* differential pseudorapidity distributions of a b-quark produced in an event with two $b\bar{b}$ pairs. One-nucleon (*dashed histograms*) and two-nucleon contributions (*continuous histograms*) in the case of a heavy (*higher histograms*) and of a light nucleus (*lower histograms*)

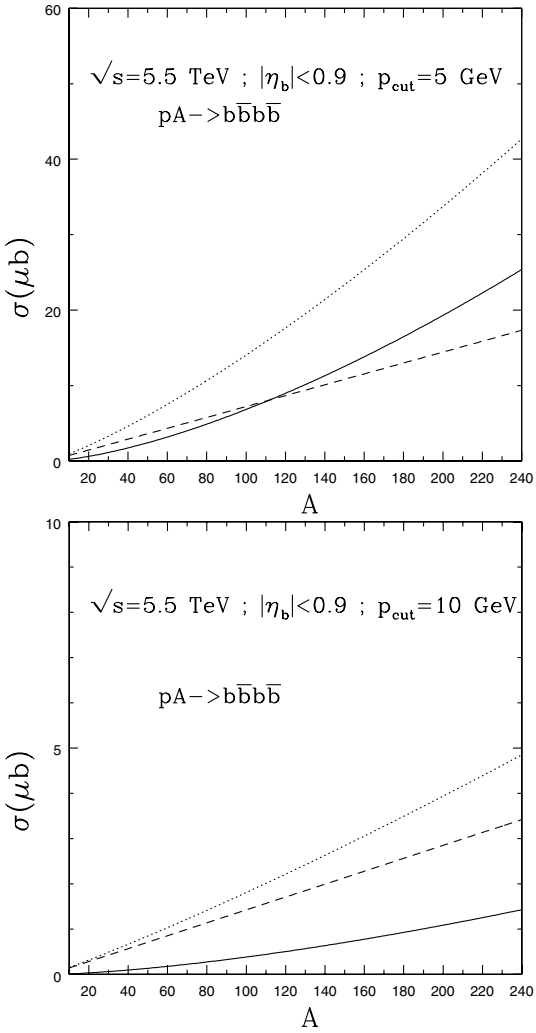

Fig. 9. Different contributions to the cross section for $b\bar{b}b\bar{b}$ production in a central calorimeter as a function of A, after applying a cut of 5 GeV (*upper figure*) and of 10 GeV (*lower figure*) in the transverse momenta of each produced b-quark: one-nucleon (*dashed line*), two nucleons (*continuous line*) processes and total (*dotted line*)

a function of the atomic mass number of the one-nucleon (dashed line) and of the two nucleons (continuous line) contributions to the cross section. The dotted line is the sum of the two terms. The lower figure shows the two contributions to the oseudorapidity distribution of a b-quark produced in an event with two $b\bar{b}$ pairs: one-nucleon (dashed histograms) and two-nucleon contributions (continuous histograms) in the case of a heavy (higher histograms) and of a light nucleus (lower histograms).

The A-dependence of the two different contributions, as a function of A, are shown in Fig. 9 in the case of a central calorimeter, after applying a cut of 5 GeV/c (upper figure) and of 10 GeV/c (lower figure) in the transverse momenta of each produced b-quark. Dashed, continuous and dotted lines have the same meaning as in Fig. 8.

The case of a forward calorimeter, $1.8 \leq \eta \leq 4.9$, is shown in Fig. 10, where the dashed, continuous and dotted lines have the same meaning as before.

Summarizing the large size of the cross section of $b\bar{b}b\bar{b}$ production in hadron-nucleus collisions at the LHC (the values are of the order of one hundreds of μb) suggests that the production of multiple pairs of b-quarks is fairly typical at high energies, hence representing a convenient channel to study multiple parton interactions. A rather spectacular feature is the "anomalous" dependence on A. The effects induced by the presence of the nucleonic degrees of freedom in the nuclear structure are in fact not limited to the usual shadowing corrections to the nuclear structure functions, which cause a limited *decrease* (not larger than 20%, in the kinematical regime considered here) of the cross section for a hard interaction in hadron-nucleus collisions. When considering double parton scatterings, all

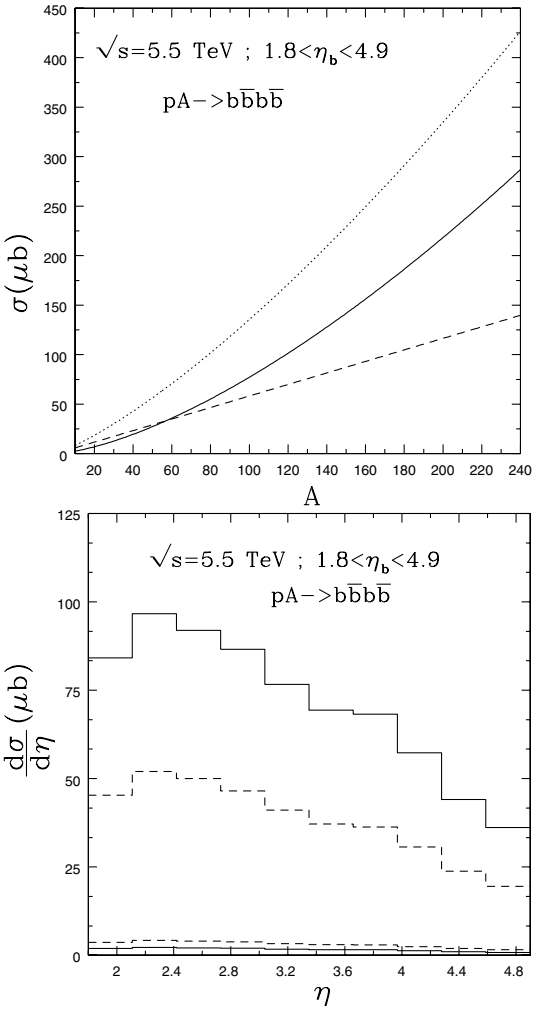

Fig. 10. Different contributions to the cross section for $b\bar{b}b\bar{b}$ production, in a forward calorimeter. Upper figure: cross section as a function of A of the one-nucleon (*dashed line*) and of the two nucleons (*continuous line*) contributions. The dotted line is the sum of the two terms. Lower figure: differential rapidity distributions of a b-quark produced in an event with two $b\bar{b}$ pairs. One-nucleon (*dashed histograms*) and two-nucleon contributions (*continuous histograms*) in the case of a heavy (*higher histograms*) and of a light nucleus (*lower histograms*)

nuclear effects are exhausted in the shadowing corrections only in the $\sigma_A^D|_1$ term. The dominant effect of the nuclear structure is on the contrary due to the presence of the $\sigma_A^D|_2$ term in the cross section, which scales with a different power of A as compared to single scattering term, giving rise to a sizably larger correction, with opposite sign as compared to shadowing correction, namely to an *increase* of the cross section which becomes sizably larger than 100% in the case of a heavy nucleus.

Acknowledgements. This work was partially supported by the Italian Ministry of University and of Scientific and Technological Researches (MIUR) by the Grant COFIN2001.

References

1. B. Anderson et al. [Small x Collaboration]: arXiv:hep-ph/0204115
2. B. Abbott et al. [D0 Collaboration]: collisions at s**(1/2) = 1.8-TeV," Phys. Lett. B **487**, 264 (2000) [arXiv:hep-ex/9905024]
3. P. Nason, S. Dawson, and R.K. Ellis: Collisions, Nucl. Phys. B **303**, 607 (1988); Nucl. Phys. B **327**, 49 (1989)
4. S. Catani, M. Ciafaloni, and F. Hautmann: Nucl. Phys. B **366**, 135 (1991)
5. J.C. Collins and R.K. Ellis: Nucl. Phys. B **360**, 3 (1991)
6. L.V. Gribov, E.M. Levin, and M.G. Ryskin: Phys. Rept. **100**, 1 (1983)
7. Y.M. Shabelski and A.G. Shuvaev: experimental data, arXiv:hep-ph/0107106
8. M.G. Ryskin, A.G. Shuvaev, and Y.M. Shabelski: beauty hadroproduction, Phys. Atom. Nucl. **64**, 1995 (2001) [Yad. Fiz. **64**, 2080 (2001)] [arXiv:hep-ph/0007238]
9. S. Catani, M. Dittmar, D.E. Soper, W. James Stirling, S. Tapprogge, S. Alekhin, P. Aurenche, C. Balazs, R.D. Ball, G. Battistoni, E.L. Berger, T. Binoth, R. Brock, D. Casey, G. Corcella, V. Del Duca, A. Del Fabbro, A. De Roeck, C. Ewerz, D. de Florian, M. Fontannaz, S. Frixione, W.T. Giele, M. Grazzini, J.P. Guillet, G. Heinrich, J. Huston, J. Kalk, A.L. Kataev, K. Kato, S. Keller, M. Klasen, D.A. Kosower, A. Kulesza, Z. Kunszt, A. Kupco, V.A. Ilyin, L. Magnea, Michelangelo L. Mangano, Alan D. Martin, K. Mazumdar, P. Mine, M. Moretti, W.L. van Neerven, G. Parente, D. Perret-Gallix, E. Pilon, A.E. Pukhov, I. Puljak, J. Pumplin, E. Richter-Was, R.G. Roberts, G.P. Salam, M.H. Seymour, N. Skachkov, A.V. Sidorov, H. Stenzel, D. Stump, R.S. Thorne, D. Treleani, W.K. Tung, A. Vogt, B.R. Webber, M. Werlen, and S. Zmouchko: CERN-TH-2000-131, May 2000. p. 115 In *Geneva 1999, Standard model physics (and more) at the LHC* 1-115 arXiv:hep-ph/0005025
10. P.V. Landshoff and J.C. Polkinghorne: Phys. Rev. D **18**, 3344 (1978); Fujio Takagi: Phys. Rev. Lett. **43**, 1296 (1979); C. Goebel, F. Halzen, and D.M. Scott: Phys. Rev. D **22**, 2789 (1980); N. Paver and D. Treleani: Nuovo Cimento A **70**, 215 (1982); B. Humpert: Phys. Lett. B **131**, 461 (1983); M. Mekhfi: Phys. Rev. D **32**, 2371 (1985), ibid. D **32**, 2380 (1985); B. Humpert and R. Odorico: Phys. Lett. **154B**, 211 (1985); T. Sjostrand and M. Van Zijl: Phys. Rev. D **36**, 2019 (1987); F. Halzen, P. Hoyer, and W.J. Stirling: Phys. Lett. **188B**, 375 (1987); M. Mangano: Z. Phys. C **42**, 331 (1989); R.M. Godbole, Sourendu Gupta, and J. Lindfors: Z. Phys. C **47**, 69 (1990)
11. M. Rosina, D. Janc, D. Treleani, and A. Del Fabbro: AIP Conf. Proc. **660**, 377 (2003) [arXiv:hep-ph/0301136]
12. D. Janc, M. Rosina, D. Treleani, and A. Del Fabbro: Few Body Syst. Suppl. **14**, 25 (2003) [arXiv:hep-ph/0301115]
13. A. Del Fabbro and D. Treleani: Phys. Rev. D **66**, 074012 (2002) [arXiv:hep-ph/0207311]
14. M.A. Kimber, A.D. Martin, and M.G. Ryskin: Eur. Phys. J. C **12**, 655 (2000) [arXiv:hep-ph/9911379]
15. G. Marchesini and B.R. Webber: Radiation, Nucl. Phys. B **310**, 461 (1988)
16. J. Blumlein: Report No. DESY 95-121, hep-ph/9506403
17. S.P. Baranov and N.P. Zotov: Hera, Phys. Lett. B **458**, 389 (1999)
18. M. Gluck, E. Reya, and A. Vogt: Z. Phys. C **67**, 433 (1995)

19. A.D. Martin, R.G. Roberts, W.J. Stirling, and R.S. Thorne: Eur. Phys. J. C **14**, 133 (2000)
20. V.D. Barger, A.L. Stange, and R.J. Phillips: Phys. Rev. D **44**, 1987 (1991)
21. A. Del Fabbro and D. Treleani: Phys. Rev. D **63**, 057901 (2001) [arXiv:hep-ph/0005273]
22. T. Stelzer and W.F. Long: Comp. Phys. Comm. **81**, 357 (1994)
23. E. Murayama, I. Watanabe, and K. Hagiwara, HELAS: HELicity Amplitude Subroutines for Feynman Diagram Evaluations, KEK report 91-11, January 1992
24. G.P. Lepage: J. Comput. Phys. **27**, 192 (1978)
25. G. Calucci and D. Treleani: Phys. Rev. D **60**, 054023 (1999)
26. T. Akesson et al. [Axial Field Spectrometer Collaboration]: Z. Phys. C **34**, 163 (1987)
27. F. Abe et al. [CDF Collaboration]: 1.8-TeV, Phys. Rev. Lett. **79**, 584 (1997)
28. F. Abe et al. [CDF Collaboration]: Phys. Rev. D **56**, 3811 (1997)
29. M. Strikman and D. Treleani: Phys. Rev. Lett. **88**, 031801 (2002) [arXiv:hep-ph/0111468]
30. N. Paver and D. Treleani: Nuovo Cim. A **70**, 215 (1982)
31. M. Braun and D. Treleani: Eur. Phys. J. C **18**, 511 (2001) [arXiv:hep-ph/0005078]
32. P. Amaudruz et al. [New Muon Collaboration]: Nucl. Phys. B **441**, 3 (1995) [arXiv:hep-ph/9503291]